

**Rationally Designed Singlet Sink for Glassy Polymeric  
Photon Upconverting Films**

Journal:	<i>Journal of Materials Chemistry C</i>
Manuscript ID	TC-ART-12-2023-004619.R1
Article Type:	Paper
Date Submitted by the Author:	09-Apr-2024
Complete List of Authors:	Stanciu, Sonia; University of Southern Mississippi, School of Polymer Science and Engineering Raišys, Steponas; Vilnius University Faculty of Physics, Institute of Photonics and Nanotechnology Kazlauskas, Karolis; Vilnius University, Institute of Photonics and Nanotechnology Simon, Yoan; University of Southern Mississippi, School of Polymer Science and Engineering; Arizona State University Biodesign Institute, School of Molecular Sciences

## ARTICLE

## Rationally Designed Singlet Sink for Glassy Polymeric Photon Upconverting Films

Sonia T. Stanciu,<sup>a</sup> Steponas Raišys,<sup>b</sup> Karolis Kazlauskas,<sup>b</sup> and Yoan C. Simon. <sup>\*a,c</sup>

Received 00th January 20xx,  
Accepted 00th January 20xx

DOI: 10.1039/x0xx00000x

Photon upconverting films require high overall conversion efficiencies along with a strong absorption of incident light and a low upconversion intensity threshold ( $I_{th}$ ) for their practical implementation (e.g. in solar harvesting, sensing, photocatalysis). Yet, a dichotomy has emerged whereby high quantum yields seemingly come to the detriment of reasonable absorption. To date, the highest efficiency reported in 9,10-diphenylanthracene-based (DPA) amorphous films were demonstrated at low sensitizer concentrations (0.01 wt%) due to increased back-energy transfer at higher sensitizer content. The need for alternatives that circumvent this trade-off is pressing. Herein we report the rational design and application of a novel 9-phenyl-10-(*p*-tolylethynyl)-anthracene (PTEA) singlet sink (or collector) in conjunction with a benchmark upconverting pair, *viz.* platinum (II) octaethylporphyrin (PtOEP) and DPA. By using a highly fluorescent singlet exciton sink, parasitic decay to the sensitizer is circumnavigated, thus improving the upconversion quantum yield ( $\Phi_{UC}$ ) at elevated sensitizer concentrations (0.05 wt% PtOEP) compared to previous reports - expanding the potential for more practical applications for solid-state TTA-UC systems.

### Introduction

Photon upconversion *via* sensitized triplet-triplet annihilation (TTA-UC) is a photophysical phenomenon enabling the conversion of an incident optical radiation into light of higher energy, *i.e.* *apparent* Anti-Stokes shift.<sup>1–5</sup> This feat is potentially useful in numerous applications,<sup>6</sup> ranging from photocatalysis<sup>7,8</sup> to increasing the photovoltaic efficiency past the Shockley-Queisser limit.<sup>9–11</sup> TTA-UC offers numerous advantages including the ability to operate under polychromatic, noncoherent radiation at subsolar excitation power densities ( $\sim$ mW cm<sup>-2</sup>).<sup>12,13</sup> Additionally, we can readily modify substituents on the sensitizer and annihilator to alter the position of singlet and triplet energy levels, as well as the magnitude of the energy gap ( $\Delta E_{ST}$ ).<sup>5,14</sup> The cascade of energy transfers that facilitate TTA-UC starts with the absorption of a photon by the sensitizer to form its singlet excited state (Figure 1).<sup>5,15</sup> Spin-orbit coupling engenders intersystem crossing (ISC) to the triplet manifold,<sup>16</sup> which in turn enables Dexter-type triplet-triplet energy transfer (TTET) from the sensitizer to the annihilator species, and subsequently triplet exciton diffusion between annihilators. Upon forming an encounter complex, two triplets annihilate via a biexcitonic process that theoretically produces a 1:3:5 ratio of

singlet:triplet:quintet multiplicity, respectively.<sup>17</sup> In TTA, the desired productive event is the formation of the high-energy singlet manifold capable of blue-shifted radiative decay. Purely from a statistical perspective, this implies 1/9 (=11%) probability for generating singlet states.<sup>17</sup> However, due to the energetic inaccessibility of the quintet state, the spin statistic limit can be increased to 40%.<sup>18</sup> This limit can be further exceeded by assuming access to the second triplet state, T<sub>2</sub>, for reverse ISC to S<sub>1</sub> or if the biexcitonic complex can decay back to T<sub>1</sub> on the annihilator without energy loss. These processes would allow theoretical maximum upconversion quantum yield ( $\Phi_{UC}$ ) to be reached.<sup>18,19</sup> It is worth noting that, given the biexcitonic nature of this process, the maximum attainable  $\Phi_{UC}$  is 50%.

While broad absorbance of the sensitizer facilitates efficient harvesting of polychromatic photons, overlap with the fluorescence (FL) band of the annihilator causes parasitic decay of upconverted singlets to the sensitizer *via* Förster resonance back-energy transfer (back-FRET) and/or simple emission re-absorption.<sup>20–22</sup> Long-range ( $\sim$ 10 nm) back-FRET to the sensitizer is profoundly detrimental to TTA-UC, preventing the full realization of a high  $\Phi_{UC}$ , even at exceedingly low sensitizer concentrations ( $\sim$ 0.01 wt%).<sup>22</sup> This issue is further exacerbated with higher sensitizer content. In 2016, Yanai and Kimizuka proposed the concept of a “singlet energy collector” to enhance fluorescent yields,<sup>23</sup> whereby annihilation and emission are

<sup>a</sup> School of Polymer Science and Engineering, The University of Southern Mississippi, 118 College Dr. #5050, Hattiesburg 39406, MS, USA.

<sup>b</sup> Institute of Photonics and Nanotechnology, Vilnius University, Saulėtekio Av. 3, LT-10257 Vilnius, Lithuania

<sup>c</sup> School of Molecular Sciences and Biodesign Center for Sustainable Macromolecular Materials and Manufacturing, Arizona State University, Tempe, AZ, 85281, USA. Email: yoan.simon@asu.edu

Electronic Supplementary Information (ESI) available: [details of any supplementary information available should be included here]. See DOI: 10.1039/x0xx00000x

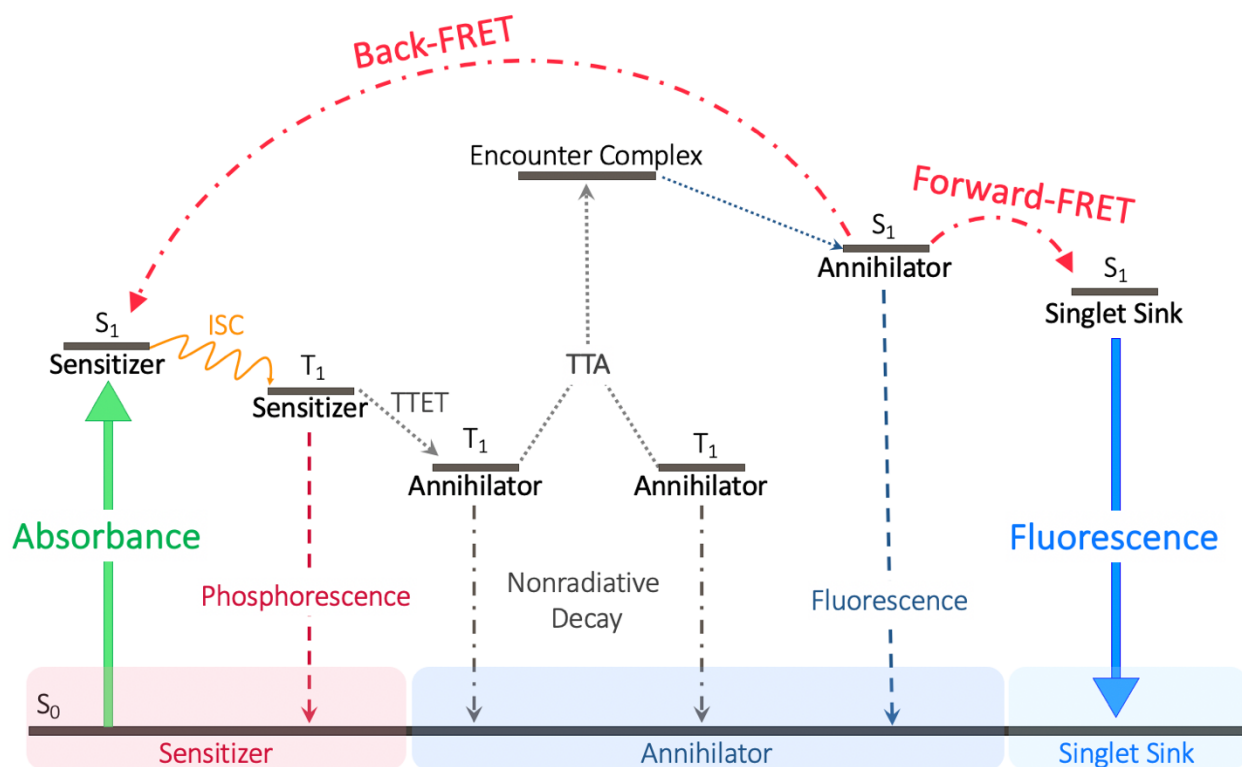


**Figure 1.** Perrin-Jablonski diagram demonstrating the idealized energy levels for photon upconversion via sensitized triplet-triplet annihilation (TTA-UC) through singlet sink approach. Intersystem crossing (ISC), triplet-triplet energy transfer (TET), triplet-triplet annihilation (TTA), Förster Resonance Energy Transfer (FRET).

decoupled by introducing a third chromophore capable of trapping the singlets generated upon TTA before parasitic decay to the sensitizer. However, using a singlet sink to increase fluorescence efficiency will inevitably reduce the apparent anti-Stokes shift, evidencing a trade-off in performance for sink-containing systems.

In 2018, Raišys et al. reported the use of 1,6-bis-[2,5-di(dodecyloxyphenyl)ethynyl]pyrene (PE) as a fluorescent “singlet-trapping sink” in poly(methyl methacrylate) (PMMA) films containing the well-documented sensitizer/annihilator pair: platinum (II) octaethylporphyrin (PtOEP) and 9,10-diphenylanthracene (DPA).<sup>22</sup> By incorporating as little as 0.01 wt% PE (PtOEP = 0.01 wt%), the  $\Phi_{UC}$  of the bulk films increased from 1.8% to 2.7%, with an upconversion intensity threshold ( $I_{th}$ ) of  $39 \text{ mW} \cdot \text{cm}^{-2}$ . Kimizuka and coworkers further examined 2,5,8,11-tetra-*tert*butylperylene (TTBP) as a “singlet energy collector” in lipophilic annihilator-based matrix-less thin films containing PtOEP, increasing  $\Phi_{UC}$  from 2.1% to 4.5% with a  $I_{th} = 195 \text{ mW} \cdot \text{cm}^{-2}$ .<sup>24</sup> Raišys et al. further expanded on the use of PE to matrix-free films of bisfluorene-anthracene (BFA) and PtOEP.<sup>25</sup> The efficiency of the BFA-methyl systems increased from  $\Phi_{UC} = 0.9\%$  at a sink loading of 0.01 wt% to  $\Phi_{UC} = 1.7\%$  at a sink loading of 0.5 wt%. In BFA-phenyl systems the efficiency was increased from  $\Phi_{UC} = 3\%$  at a sink loading of 0.01 wt% to  $\Phi_{UC} = 3.4\%$  at a sink loading of 0.1 wt%.

Herein, we report the facile synthesis of a new singlet sink: 9-phenyl-10-(*p*-tolylethynyl)-anthracene (PTEA) and its

introduction into PMMA upconverting films with PtOEP as a sensitizer and high-purity DPA as an annihilator (Figure 2).<sup>26</sup> This approach allowed us to increase the concentration of PtOEP

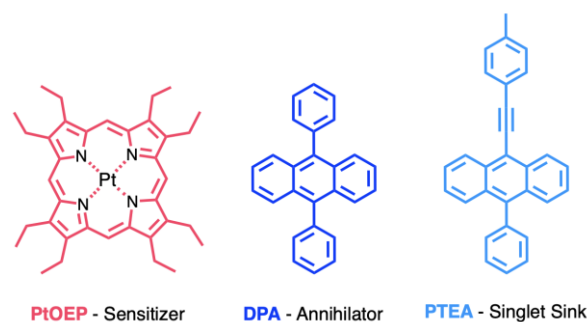


**Figure 2.** Chemical structures of platinum (II) octaethylporphyrin (PtOEP) sensitizer, 9,10-diphenylanthracene (DPA) annihilator, and 9-phenyl-10-(*p*-tolylethynyl)-anthracene (PTEA) singlet sink.

from 0.01 wt% to 0.05 wt% while successfully limiting back-FRET, thereby expanding the operational window of TTA-UC towards lower intensity incident light. Gratifyingly, we achieved a  $\Phi_{UC} = 5\%$  in glassy films containing 0.05 wt% PtOEP, 40 wt% DPA, and 0.25 wt% PTEA. Through this work, we expand the concept of a singlet sink in TTA-UC to improve the overall  $\Phi_{UC}$  while maintaining a low UC intensity threshold, ultimately broadening the scope of upconversion applications.

## Experimental

**Materials.** All reagents and solvents were purchased from commercial sources and used as received. 4-Ethynyltoluene (97% Purity): GFS Chemicals. 9-bromo-10-phenylanthracene (98% Purity), tetrakis(triphenylphosphine)palladium (0) ( $\text{Pd}(\text{PPh}_3)_4$  (98% Purity), copper (I) iodide ( $\text{CuI}$ ) (99% Purity): Ambeed, Inc. Triethylamine ( $\text{Et}_3\text{N}$ ) (99.5% Purity): Chem Impex. Tetrahydrofuran (THF) and dichloromethane (DCM): Fisher Scientific. Deuterated chloroform: Thermo Scientific. Pt (II) octaethylporphin (PtOEP): Frontier Scientific. 9,10-Diphenylanthracene (DPA) (97% Purity): Oakwood Chemical. Materials used for film fabrication: DPA (>99.0% Purity, sublimed grade): Tokyo Chemical Industry. PtOEP and Toluene: Merck. Poly(methyl methacrylate) (PMMA): Arkema. avg. molecular weight = 125 kDa. Avg.  $\bar{D}$  = 1.002.

**Synthetic Procedure for 9-phenyl-10-(p-tolylethynyl)-anthracene (PTEA).** Catalyst stock solutions were prepared first to permit stir times of minimum 1 h. In a nitrogen ( $\text{N}_2$ ) glovebox, tetrakis(triphenylphosphine)palladium (0) ( $\text{Pd}(\text{PPh}_3)_4$ , 36.96 mg, 0.032 mmol, 0.04 equiv.) catalyst was weighed into a 20-mL storage vial equipped with a pressure relief cap. Degassed THF (4 mL) stored over molecular sieves was then added to the vial. The vial was then sealed and stirred for minimum 1 h. Copper (I) iodide ( $\text{CuI}$ ) (12.18 mg, 0.064 mmol, 0.08 equiv.) cocatalyst was weighed into a 20-mL storage vial equipped with a pressure relief cap. The storage vial containing  $\text{CuI}$  was removed from the glovebox while remaining sealed under  $\text{N}_2$ . A separate 20-mL storage vial containing triethylamine ( $\text{Et}_3\text{N}$ ) was purged with argon for 15 min. Degassed  $\text{Et}_3\text{N}$  (4 mL) was then added to the vial contain  $\text{CuI}$  using a vacuum-tight syringe. The solution was stirred for minimum 1 h.

To a 100-mL round-bottom Schlenk flask sealed with a rubber screw-type septum and equipped with a magnetic stir bar, 9-bromo-10-phenylanthracene (266 mg, 0.80 mmol, 1 equiv.), 4-ethynyltoluene (122  $\mu\text{L}$ , 0.96 mmol, 1.2 equiv.) were dissolved in a THF: $\text{Et}_3\text{N}$  1:1 (v:v) solution (24 mL), after which the reagents were stirred briefly under argon atmosphere. Three freeze-pump-thaw cycles were then performed, after which the Schlenk flask was backfilled with Ar and thawed in lukewarm water and the cocatalyst and catalyst solutions were injected into the sealed reaction flask with a vacuum-tight syringe. Finally, the reaction flask was stirred in an oil bath for 4 h at 70 °C. The reaction was allowed to cool to room temperature and slowly opened to atmosphere. Then, the organic layer was concentrated under reduced pressure by rotary evaporation. The crude solid was purified by flash column chromatography (FCC) with a fixed solvent ratio of DCM:hexanes 1:9 (v:v) (product  $R_f$  = 0.46) and concentrated by rotary evaporation, producing a bright yellow powder in a yield of 37.9%.  $^1\text{H-NMR}$  ( $\text{CDCl}_3$ , 400 MHz)  $\delta$  ppm: 8.77-8.74 (d, 2H), 7.71-7.67 (t, 4H), 7.61-7.55 (m, 5H), 7.45-7.38 (m, 4H), 7.29-7.26 (d, 2H), 2.45 (s, 3H).  $^{13}\text{C-NMR}$  ( $\text{CDCl}_3$ , 151 MHz)  $\delta$  ppm: (138.70, 138.62, 138.17, 132.25, 131.60, 131.21, 129.99, 129.33, 128.40, 127.66, 127.40, 127.01, 126.24, 125.59, 120.69, 117.77, 101.25, 85.96, 21.63).

HRMS  $m/z$  [ $\text{M}^+$ ] calc. for PTEA ( $\text{C}_{29}\text{H}_{20}$ ): 369.1637777 g/mol, found, 369.163835 g/mol. UV-Vis (THF):  $\lambda_{\text{max}}$ , nm (rel. in): 303 (0.78), 407 (0.69), 430 (0.68).

**Molecular Characterization.**  $^1\text{H}$  NMR spectroscopy was performed on a Bruker Ascend 400 MHz spectrometer (Figure S1).  $^{13}\text{C}$  NMR spectroscopy was performed on a Bruker Ascend 600 MHz spectrometer (Figure S2). Residual solvent peaks were used as internal reference standards.<sup>27</sup> High-resolution mass spectrometry (HRMS) was completed using positive-ion mode electrospray ionization with an Apollo II ion source on a Bruker 10 Tesla APEX-Qe FTICR-MS.

**Thermal Studies.** Thermogravimetric analyses (TGA) were performed on a Mettler-Toledo TGA STAR instrument by heating materials from 25 to 800 °C under  $\text{N}_2$  at 10 °C /min. Decomposition temperature was taken at 10% mass loss. Differential scanning calorimetry (DSC) experiments were performed on a Mettler-Toledo STAR DSC instrument under  $\text{N}_2$  at varying ramp rates and temperature scales (*vide infra*).

**Materials Processing.** Upconverting films with a fixed sensitizer content of PtOEP = 0.05 wt% and varying singlet sink concentrations were prepared in a  $\text{N}_2$ -filled glove box. Stock solutions of toluene, DPA (50 mg/mL), PtOEP (0.1 mg/mL), and PMMA (100 mg/mL) were prepared and mixed at appropriate ratios towards a final concentration of PMMA/DPA (40 wt%)/PtOEP (0.05 wt%)/PTEA (X wt%), where X is 0, 0.025, 0.05, 0.1, 0.25 and 0.5. Here, wt% is defined as a weight percentage relative to the total weight of the system minus the toluene. The solutions were drop-casted onto microscope cover glass slides (15 × 15 mm, 150  $\mu\text{m}$  thick) that had been pre-cleaned. The pre-cleaning process involved sonicating the slides in a 1% v/v Hellmanex III aqueous solution at 65 °C for 15 min, followed by rinsing with deionized water five times after sonication. The drop-casting was performed at  $\sim 100$  °C, and the slides were left to dry for  $\sim 1$  hour.

Aluminum foil spacers (15 × 15 mm, 50  $\mu\text{m}$  thick) with a 12 mm diameter cut-out aperture were positioned between two glass slides (15 × 15 mm, 150  $\mu\text{m}$  thick and 18 × 18 mm, 150  $\mu\text{m}$  thick) in a custom-made mechanical hot-press (Figure S3). The films were melted at 260 °C for 1 min and then maintained under slight pressure for an additional 1 min, resulting in the formation of smooth  $\sim 50$   $\mu\text{m}$ -thick polymeric films sandwiched between glass slides. Subsequently, the films were rapidly cooled to room temperature on a metal surface. Finally, the prepared films were encapsulated by epoxy resin inside the glove box prior to conducting photophysical measurements in ambient conditions. Films for fluorescence concentration quenching experiments were prepared under identical conditions, except that they were drop-cast at room temperature in ambient air and were not encapsulated after melt-processing.

**Optical Experiments.** The UV-vis absorption spectra of PTEA and other chromophores were measured in THF solutions ( $c = 0.016$  mg/mL) with a Perkin Elmer Lambda 35 UV/Vis Spectrometer from 240 to 800 nm. Photoluminescence spectra of PTEA in THF were measured by exciting at 405 nm (LED emitter) at an angle of  $90^\circ$  to the incident light with a Horiba Scientific spectrofluorometer by a solution prepared in THF at 0.5 mg/mL. Photoluminescence spectra of DPA in THF were measured in identical conditions by exciting at 375 nm. The fluorescence quantum yield ( $\Phi_{\text{FL}}$ ) of PTEA in THF was measured at a concentration of  $10^{-5}$  M a Horiba Scientific K-Sphere by exciting at 405 nm at a  $90^\circ$  angle geometry.

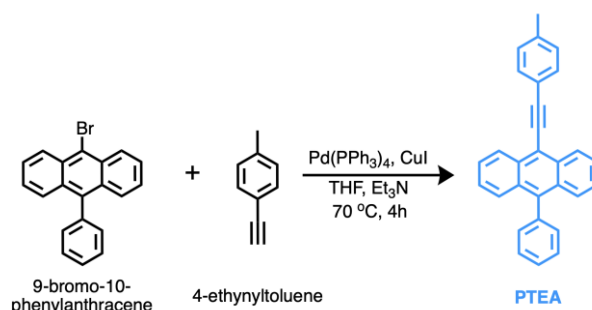
The fluorescence of the polymer films was excited at 370 nm using a 150-W xenon arc lamp (LOT-Oriel) coupled to a monochromator (Sciencetech Inc.), whereas UC emission was induced by exciting at 532 nm using continuous-wave semiconductor laser diode (Integrated Optics). Emission was measured with a back-thinned CCD spectrometer PMA-12 (Hamamatsu). The fluorescence and UC emission quantum yields were estimated by utilizing an integrating sphere (Sphere Optics) coupled to the same CCD spectrometer via an optical fiber.<sup>28</sup> Fluorescence transients at peak emission wavelength of the films were measured by using a time-correlated single-photon counting system PicoHarp 300 (PicoQuant), which utilized a pulsed semiconductor laser diode (repetition rate - 2.5 MHz, pulse duration - 70 ps, emission wavelength - 375 nm, PicoQuant) as an excitation source. UC transients were recorded using a time-gated intensified CCD camera New iStar DH340T (Andor) coupled to a spectrograph SR-303i (Shamrock). In these experiments, frequency-doubled pulsed Nd<sup>3+</sup>:YAG laser (Ekspla) (wavelength - 532 nm, pulse duration - 5 ns, repetition rate - 20 Hz) served as an excitation source. All photophysical measurements were performed at room temperature except determination of the PTEA phosphorescence, which was measured in a closed-cycle helium cryostat 204N (Cryo Industries of America) at a temperature of 15 K.

## Results and Discussion

**Synthesis and characterization of 9-phenyl-10-(*p*-tolylethynyl)-anthracene (PTEA).** To decouple the annihilation and emission mechanism, it is necessary to develop an efficient singlet sink with a high fluorescence quantum yield ( $\Phi_{\text{FL}}$ ), as well as a singlet energy only slightly lower than that of the annihilator to ensure preferential forward-FRET to the sink without a significant reduction in apparent anti-Stokes shift.<sup>22,25</sup> Additionally, the triplet energy of the sink should be higher than that of the annihilator to avoid the premature depopulation of triplets before TTA. Lastly, it is preferential if the singlet lifetime of the sink is shorter than that of the annihilating species to ensure rapid emission from the singlet sink, rather than back-FRET to the sensitizer. Overall, these stringent conditions impose meticulous architectural design of the singlet sink to enhance TTA-UC.

We thus designed a novel polycyclic aromatic hydrocarbon (PAH) around an anthracene core with extended conjugation compared to

that of DPA. To this end, we performed a Pd-catalyzed Sonogashira coupling of 9-bromo-10-phenylanthracene and 4-ethynyltoluene to obtain PTEA (Scheme 1).<sup>29</sup> We observed the formation of PTEA by monitoring the disappearance of the alkyne proton at 3.05 ppm, as well as a downshift of the aromatic protons closest to the bromo unit



**Scheme 1.** Synthesis of 9-phenyl-10-(*p*-tolylethynyl)-anthracene (PTEA) singlet sink by Sonogashira cross-coupling of 9-bromo-10-phenylanthracene and 4-ethynyltoluene.

from 8.63-8.61 ppm to 8.77-8.74 ppm (Figure S2). Absorbance and emission of PTEA in dilute conditions were characterized by UV-vis and fluorescence spectroscopy to confirm the successful synthesis of a highly emissive anthracene-type PAH. In THF, PTEA exhibits an absorption maximum at 407 nm (3.05 eV), with a molar extinction coefficient (MEC) of  $2.30 \cdot 10^4$  M<sup>-1</sup> cm<sup>-1</sup>, a second intense vibronic band at 430 nm (2.88 eV), as well as a two less-intense vibronic bands at 418 and 386 nm (Figure S4). The absorbance profile of DPA demonstrates similar vibronic replicas, characteristic of its anthracene core (Figure S5).<sup>30</sup> PTEA exhibits an emission maximum in THF ( $c = 10^{-5}$  M) at 443 nm (2.80 eV), a less intense vibronic band at 456 nm, and a second, intense vibronic band at 469 nm (2.64 eV) upon excitation at 375 nm (Figure 3). Additionally, PTEA exhibits a  $\Phi_{\text{FL}} = 96.3\%$  (Figure S6); which compares favorably to the measurements of previously reported sinks in dilute solutions (PE  $\Phi_{\text{FL}} = 75\%$ , TTBP = 88.9%).<sup>22,24</sup> PTEA displays similar spectral properties to previously reported 9-(4-phenylethynyl)-10-phenylanthracene (PEAP),<sup>31</sup> albeit with a higher  $\Phi_{\text{FL}}$  (96.3% versus 79%  $\pm$  6), a red shift in emission maxima, and a methyl group **added to attempt to limit the formation of edge-to-face aggregates**.<sup>32</sup> Gratifyingly, the favorable spectral overlap between DPA emission (DPA emission maxima = 430 nm) and PTEA absorption should promote forward-FRET to the sink (Figure 3).

We calculated the overlap integral,  $J$ , for PTEA emission  $\rightarrow$  PtOEP absorption and DPA emission  $\rightarrow$  PtOEP absorption in PMMA films containing 0.05 wt% PtOEP, 40 wt% DPA, and varying concentrations (0 – 0.5 wt%) of PTEA. We determined that while  $J$  is larger for PTEA ( $J_{\text{PTEA}} = [1.8-2.1] \cdot 10^8$  nm<sup>6</sup>, versus  $J_{\text{DPA}} = 1.5 \cdot 10^8$  nm<sup>6</sup>), the significantly lower concentration of PTEA should promote a decreased back-FRET rate to PtOEP compared to that of DPA  $\rightarrow$  PtOEP (see Figure S7, Table S1 and explanation therein).

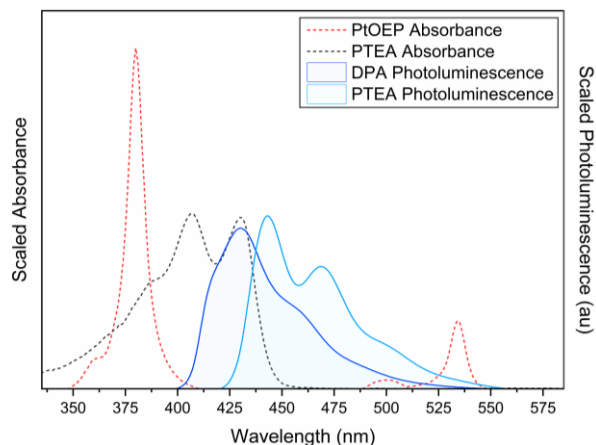


**Figure 3.** Absorbance of PtOEP (dashed red line) and PTEA (dashed grey line) and photoluminescence spectra (a.u.) of DPA (dark blue) and PTEA (light blue). Absorbance measurements in THF at  $c \approx 4 \cdot 10^{-5}$  M; Photoluminescence measurements for DPA in THF at  $c \approx 1 \cdot 10^{-3}$  M. Photoluminescence measurements for PTEA in THF at  $c \approx 1 \cdot 10^{-5}$  M. DPA and PTEA excitation at 375 nm. The spectra are scaled for clarity.

Thermogravimetric analysis (TGA) was utilized to determine a stable temperature range for processing. PTEA exhibits a decomposition temperature defined by 10% mass loss at approximately 410 °C, indicating higher thermal robustness than DPA (decomposition at approximately 322 °C) (Figure S8). The crystallization and melt dynamics of PTEA are far more complicated than that of DPA, varying broadly with increasing heating and cooling rates during differential scanning calorimetry (DSC). While DPA and PtOEP display singular crystallization peaks (94 and 23 °C, respectively) and melt peaks (241 and 323 °C, respectively), PTEA demonstrates molecular glass-like behavior, with a glass transition temperature around 45 °C in the bulk regardless of the heating/cooling rates and significant cold crystallization upon heating (Figure S9). The multiple melt peaks of PTEA, which range broadly from approx. 151 °C (ramp rate of 5 °C/min) to 192 °C (ramp rate of 10 °C/min) are indicative of polymorphic behavior.<sup>33,34</sup> We propose that this unique cold crystallization and melt behavior arises from the asymmetry of PTEA compared to DPA.<sup>27</sup> Interestingly, this behavior is consistent with the well-documented formation of anthracene excimers, which we also observed (*vide infra*).<sup>30</sup>

The efficacy of PTEA as a triplet annihilator for PtOEP was evaluated by studying the photoluminescence of PtOEP in solution upon increasing PTEA concentration (Figure S10). Upon excitation of the Q-band (532 nm), the photoluminescence intensity at the phosphorescence maxima of PtOEP (645 nm) displayed a continuous decrease with increasing PTEA concentration. Additionally, excitation at the Q-band of PtOEP resulted in an anti-Stokes-like emission maxima at 470 nm, with an increase in photoluminescence intensity upon increasing PTEA content. The decrease in photoluminescence intensity at 645 nm, combined with the increase in photoluminescence intensity at 470 nm, indicates that solution-state PTEA/PtOEP TTA-UC is achievable.

Unfortunately, application of PTEA as an annihilator for solid-state upconversion is deterred by its strong tendency to form red-shifted aggregates/excimers (Figure 4a). Aggregation of PTEA past 1 wt%

load in PMMA leads to a distinct redshift in emission maxima nearing the Q-band of PtOEP. The spectral shift in Figure 4a upon increasing PTEA concentration is not solely due to re-absorption (self-filtering) because of concomitantly observed significant lifetime shortening (Figure S11). Fluorescence lifetime shortening indicates the tendency for FRET to the lower energy PTEA aggregates. Additionally, the change in the long-wavelength slope of the absorbance-corrected fluorescence (FL) spectra (Figure S12) suggests energy transfer to lower-lying states via FRET. Ground state absorption spectra of PMMA films with increasing PTEA concentration were measured (Figure S13). For films containing 10 wt% PTEA and higher, the enhanced light scattering necessitated the use of an integrating sphere module. However, despite observing clear aggregates via

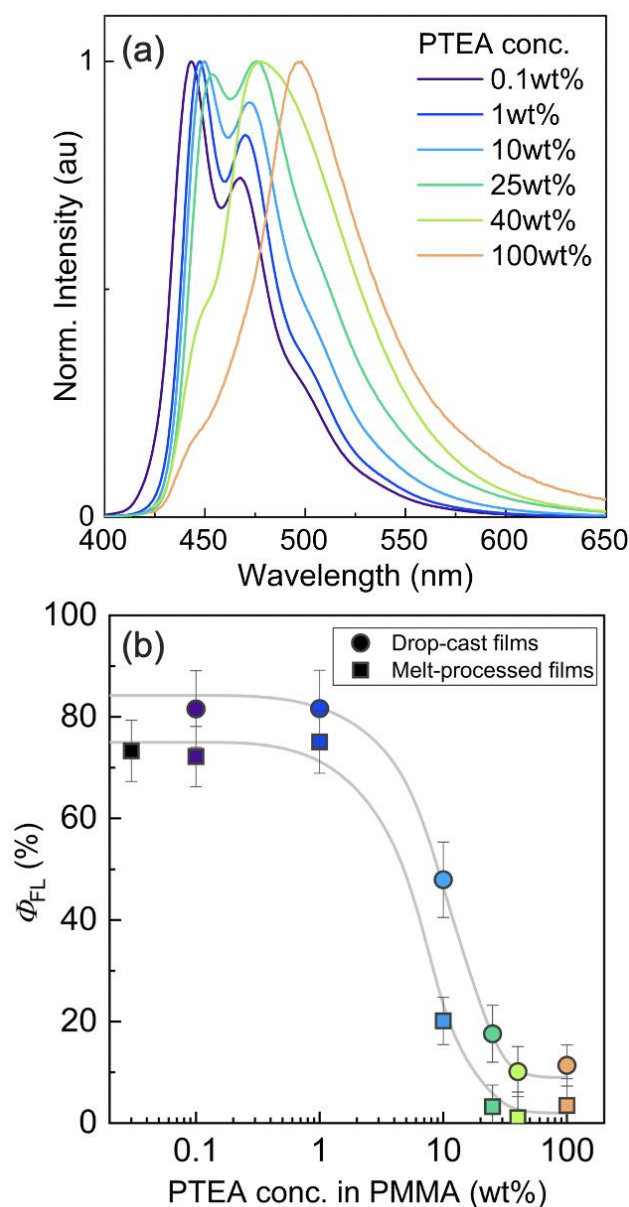


**Figure 4.** (a) Normalized emission intensity of drop-cast PMMA films doped with increasing concentrations of PTEA upon excitation at 370 nm (b) Fluorescence quantum yield ( $\Phi_{FL}$ ) of drop-cast (circles) and melt-processed (squares) PMMA films with increasing PTEA concentration. Note the symbols are color-coded to match the concentrations in Figure 4a. All films in Figure 4 a and b are DPA-free.

optical microscopy (Figure S14), the increased background signal due to light scattering hindered the detection of distinct aggregate bands in the absorption spectra. The optical microscopy spectra, paired with the redshift in Figure 4a, means a potential contribution from excimer species cannot be ruled out. Despite being antagonistic to the nature of a solid-state annihilator, the tendency of PTEA to form excimers could prove interesting in multistimuli-responsive systems.

The FL concentration quenching experiments on PMMA films doped with PTEA indicate that the successful monomolecular properties of PTEA should be maintained up to 1 wt%, encouraging efficient trapping of the singlet excitons towards improved UC performance (Figure S11 and Table S2). Compared to DPA, which displays a singlet lifetime  $\tau = 11$  ns in PMMA,<sup>22</sup> the PTEA FL lifetime was approximately half, viz.  $\tau = 5.5$  ns below 1 wt%. This decay rate is paramount to ensure preferential decay from the singlet sink.<sup>21</sup> While PTEA concentrations below 1 wt% exhibit the same mono-exponential decay, further increase in the concentration of PTEA leads to multi-exponential behavior with a significant decrease in  $\tau$  down to 1.91 ns for films with 40 wt% of PTEA. Films containing 100 wt% PTEA display a surprisingly large  $\tau = 4.13$  ns, likely due to formation of the longer-lived excimer emission.

The  $\Phi_{FL}$  of drop-cast films with increasing concentrations of PTEA were measured using an integrating sphere upon excitation at 370 nm (Figure 4b), reaching 82% for the films with PTEA concentration up to 1 wt%. Further increasing PTEA concentration past the aggregation onset lowers the  $\Phi_{FL}$  down to ca. 10%, likely due to increased non-radiative decay for the aggregates/excimers or diffusion-assisted exciton trapping at deactivation sites. Interestingly, the melt-processed films exhibit a slightly lower  $\Phi_{FL}$  at all concentrations compared to the drop-cast films (Figure 4b), which we attribute to potential oxidation of the chromophores upon melt-

processing under ambient conditions, and/or the formation of exciton-trapping defects.<sup>26</sup>

**TTA-UC via singlet sink approach.** While many parameters play a role in the effective implementation of TTA-UC, a high upconversion quantum yield ( $\Phi_{UC}$ ) is one of the most important factors for high-performance UC systems. The quantitative definition of  $\Phi_{UC}$  is established in Equation 1:

$$\Phi_{UC} = \frac{1}{2} f \Phi_{ISC} \Phi_{TTET} \Phi_{TTA} \Phi_{FL} \quad (1)$$

where  $\Phi_{ISC}$ ,  $\Phi_{TTET}$ ,  $\Phi_{TTA}$ ,  $\Phi_{FL}$ , are the quantum yields for the ISC, TTET, TTA, and emitter photoluminescence, respectively.<sup>5</sup> The  $f$  indicates the probability with which annihilation will produce the desired excited singlet state (the spin statistical limit), and the  $\frac{1}{2}$  denotes the biexcitonic nature of TTA-UC. Until now, TTA-UC in doped glassy polymer films has been restricted to low sensitizer concentrations (~0.01 wt%) on account of elevated back-FRET.<sup>22,35–39</sup> Sink-free sensitizer/annihilator upconverting films consisting of 0.05 wt% PtOEP and 40 wt% DPA display remarkably low  $\Phi_{FL} = 18\%$  and  $\Phi_{UC} = 2.7\%$  (Figure 5a and b), despite the high  $\Phi_{FL} = 85\%$  of pure DPA in PMMA films.<sup>40</sup> The lower quantum yields, as compared to those obtained by Raišys et al<sup>26</sup> at an identical annihilator concentration, is likely a result of increased back-FRET when increasing sensitizer content from 0.01 wt% to 0.05 wt%. To more thoroughly evaluate why the sink-free UC films were less efficient than the ones reported previously,<sup>26</sup> we compared emission properties as a function of film thickness to rule out thickness-induced re-absorption. Both re-absorption and back-FRET depend on concentration of the chromophores, as well as spectral overlap – however, only back-FRET would significantly alter emission lifetime. In our previous work<sup>26</sup> and the current study, films containing 40 wt% DPA have a similar thickness of around 50  $\mu\text{m}$ . The 5-fold higher sensitizer

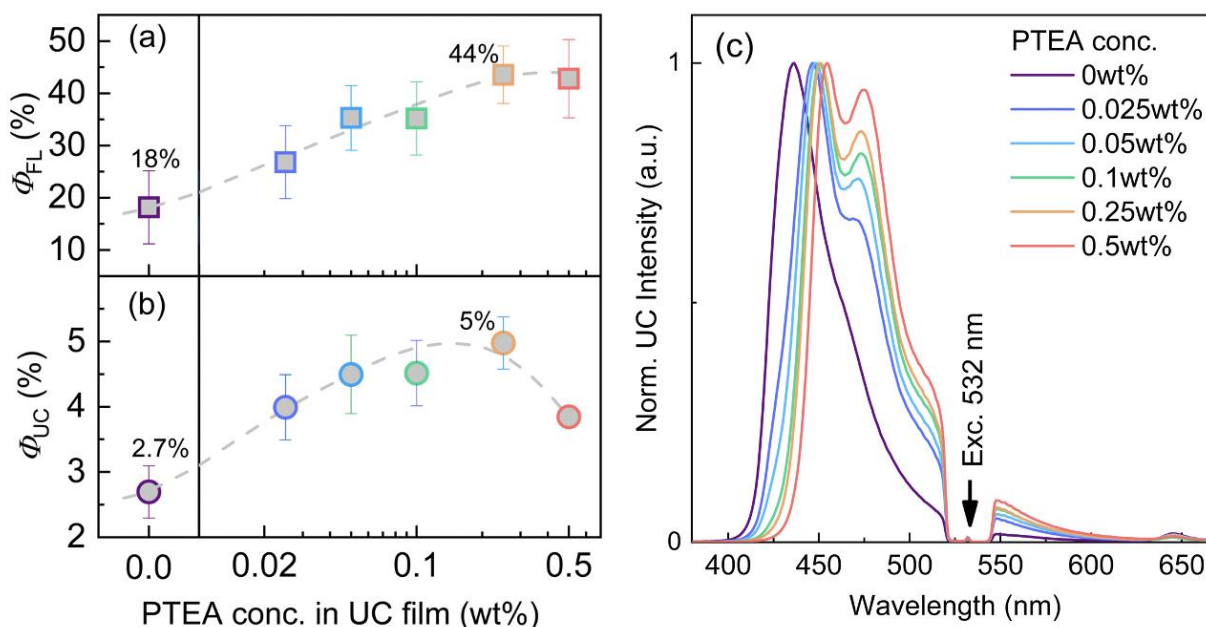


**Figure 5.** (a) FL and (b) UC quantum yield of melt-processed PMMA films containing 40 wt% DPA, 0.05 wt% PtOEP and increasing PTEA concentration. FL and UC excitation wavelengths, 370 nm and 532 nm, respectively. Dashed lines are guides to the eye. (c) Normalized UC spectra with increasing PTEA concentration, obtained using 532 nm notch filter. All UC quantum yield measurements performed at an excitation power density of  $2 \text{ W} \cdot \text{cm}^{-2}$  to ensure excitation well exceeding  $I_{th}$ .

concentration utilized in this work coincides with a significant shortening in fluorescence lifetime of DPA in sink-free films (Figure S15). This decrease in fluorescence lifetime strongly supports the proclivity for back-FRET to PtOEP. To further substantiate the negligible role of re-absorption, we fabricated sink-free PMMA films with 40 wt% DPA and 0.05 wt% PtOEP at varying thicknesses ranging from approximately 10  $\mu\text{m}$  to 200  $\mu\text{m}$ . The minimal changes in both their FL spectrum (Figure S16a) and lifetime (Figure S16b) across varying film thicknesses supports the negligible role of re-absorption due to film thickness.

By holding sensitizer and annihilator concentration steady, the introduction of 0.025 wt% PTEA into the films led to a rapid increase in both  $\Phi_{\text{FL}}$  and  $\Phi_{\text{UC}}$  to 27% and 4%, respectively. A further 10-fold increase in the concentration of PTEA (to 0.25 wt%) resulted in maximum values for  $\Phi_{\text{UC}}$  and  $\Phi_{\text{FL}}$ , 5% and 44%, respectively, *viz.* approximately two-fold higher compared to those of sink-free films. The UC emission maximum for sink-free films was observed at 430 nm (Figure 5c), matching that of pure DPA in THF. The introduction of 0.025 wt% PTEA resulted in a shift of the emission maximum to 445 nm, with a further red-shift observed with increasing PTEA content. This red-shift, along with the observed relative intensity increase of the 470 nm vibronic band, can be attributed to enhanced re-absorption. Bulk-like excitation achieved via the sensitizer at 532 nm promotes this effect by creating a longer path length for emitted UC photons to undergo re-absorption.

The unfiltered true-color pictures of UC films exposed to 532 nm excitation are displayed in Figure S17, with visible brightening when comparing sink-free UC films to 0.25 wt% PTEA-doped UC films. Unfortunately, even below the onset of aggregation for the sink, at higher PTEA concentrations the  $\Phi_{\text{UC}}$  and  $\Phi_{\text{FL}}$  began to decrease or saturate (Figure 5a and b), which we attribute to back-FRET from PTEA to PtOEP at elevated sink concentrations – as reported previously.<sup>22,25</sup>

To demonstrate the reduced back-FRET of PTEA  $\rightarrow$  PtOEP compared to DPA  $\rightarrow$  PtOEP, we fabricated two sets of PMMA films: one containing 40 wt% DPA and another containing 0.25 wt% PTEA (the PTEA concentration at which the highest  $\Phi_{\text{UC}}$  was achieved in this work). Both sets of systems incorporated increasing concentrations of PtOEP (0.01 wt% - 0.2 wt%). Stern-Volmer quenching analysis yielded Stern-Volmer constants ( $K_{\text{SV}}$ ) of  $2.0 \cdot 10^2 \text{ M}^{-1}$  for 0.25 wt% PTEA and  $3.09 \cdot 10^3 \text{ M}^{-1}$  for 40 wt% DPA (Figure 6, Figure S18).

Crucially, UC films employed in this study contain a 160-fold higher concentration of DPA compared to PTEA. Consequently, back-FRET from 40 wt% DPA  $\rightarrow$  PtOEP is considerably greater, with  $K_{\text{SV}}$  one order of magnitude higher, contributing to a stronger overall quenching effect.

As predicted by the strong overlap in DPA emission with PTEA absorbance (Figure 3), the forward-FRET of upconverted singlets from DPA to PTEA will occur even at low sink concentrations. The forward-FRET was evaluated from fluorescence transients of the UC films measured at the DPA-dominating emission band at  $\sim 410 \text{ nm}$  (Figure S19, Table S3). While the forward-FRET efficiency ( $\Phi_{\text{F-FRET}}$ ) is relatively low  $\sim 39\%$  at 0.025 wt% PTEA (Figure 7), it increases significantly, reaching almost 75% at 0.1 wt% PTEA, ultimately reaching nearly 90% at 0.5 wt% PTEA. The high  $\Phi_{\text{F-FRET}}$ , combined with

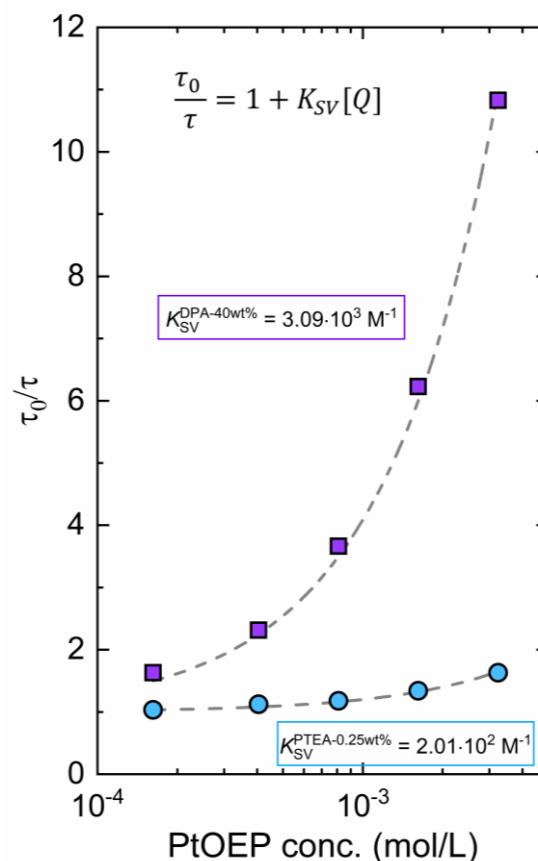


**Figure 6.** Stern-Volmer plot of emission quenching for PMMA films with varying PtOEP molar concentration. PMMA density averaged to 1.18  $\text{g}/\text{cm}^3$ .<sup>46</sup>  $\tau_0$  = singlet lifetime without presence of quencher (Q).  $\tau$  = singlet lifetime in the presence of Q.

the red-shift in UC emission spectra (Figure 5c), indicates that dual emission from the annihilator and the sink occurs at low singlet sink loads. Meanwhile, higher PTEA doping concentrations led to the predominance of radiative decay from the sink. While we still cannot fully decouple the annihilation and emission step, DPA emission is greatly reduced upon introduction of purpose-designed sinks, despite its concentration being  $\sim 80$  times higher than that of PTEA.

The elucidation of proper excitation conditions was critical to obtain accurate  $\Phi_{\text{UC}}$  values. While  $\Phi_{\text{UC}}$  is impacted by annihilator concentration, it also depends on the overall excitation power density of an UC system. Upon excitation by a continuous source, TTA-UC emission intensity displays a quadratic dependence at lower excitation densities and a linear dependence at higher excitation densities.<sup>41</sup> This shift from quadratic-to-linear dependence, referred to as the UC intensity threshold ( $I_{\text{th}}$ ), corresponds to the steady-state excitation intensity in which half of all annihilator triplets become depopulated *via* TTA mechanism, with  $\Phi_{\text{UC}}$  reaching half of its system-dependent maximum value.<sup>42</sup> Quantifying  $I_{\text{th}}$  is extremely important because  $\Phi_{\text{UC}}$  measurements must be performed in a regime where  $I \gg I_{\text{th}}$ , otherwise,  $\Phi_{\text{UC}}$  is limited by the excitation power density given to the sensitizer. When studies are run at significantly higher excitation than  $I_{\text{th}}$  the triplet population is no

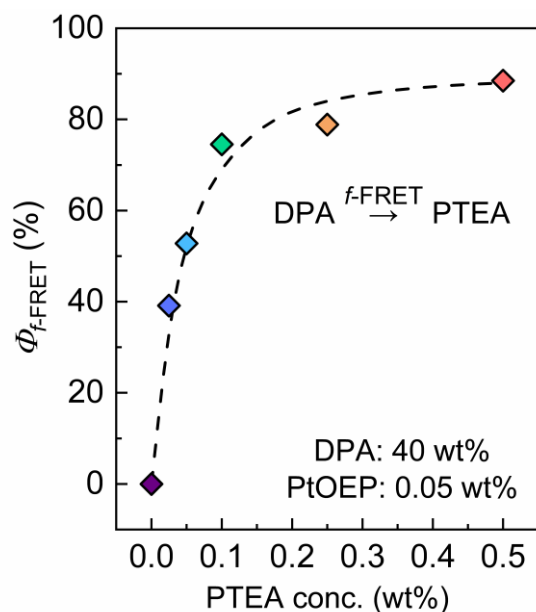


**Figure 7.** Estimated forward-FRET efficiency versus PTEA concentration in upconverting PMMA films containing 0.05 wt% PtOEP and 40 wt% DPA. Dashed line is a guide to the eye. Excitation: 532 nm. Further details in Figure S19 and Table S3.

longer dependent on energy entering the system, but rather how quickly the sensitizer can perform ISC and TTET.<sup>40–43</sup> We systematically investigated the quadratic-to-linear UC intensity shift of increasing PTEA concentrations as a function of excitation power density (Figure S20), determining the  $I_{th}$  for each film (Figure 8).

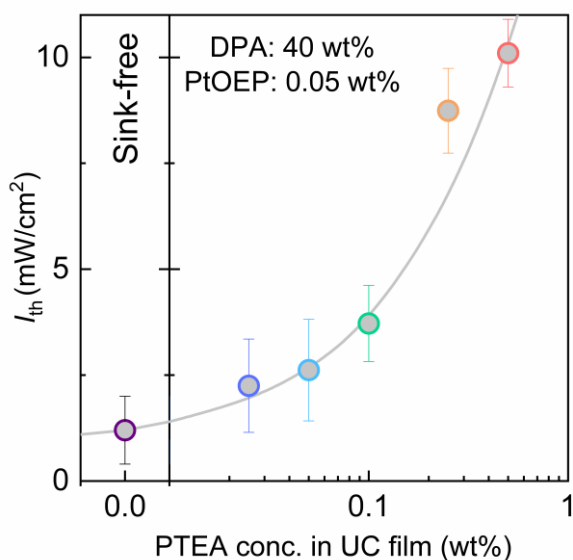


**Figure 8.** UC intensity threshold as a function of PTEA concentration in UC film (for evaluation of  $I_{th}$  see Figure S20). Excitation wavelength: 532 nm. Error bars represent uncertainty from two sources: i) the distribution of measurement values obtained at different locations on the same film, and ii) the fitting error associated with the UC intensity vs excitation density relationship.

While the sink-free PMMA films containing 0.05 wt% PtOEP and 40 wt% DPA display a relatively low  $I_{th}$  of  $1.2 \text{ mW} \cdot \text{cm}^{-2}$ , the addition of 0.025 wt% PTEA prompts a slight increase to  $I_{th} = 2.25 \text{ mW} \cdot \text{cm}^{-2}$ .  $I_{th}$  continues to rise with increasing PTEA concentrations up to  $I_{th} \approx 10 \text{ mW} \cdot \text{cm}^{-2}$  at sink loads just below the PTEA aggregation onset. For comparison, the previously reported  $I_{th}$  values for other singlet-sink systems were  $39 \text{ mW} \cdot \text{cm}^{-2}$  and  $195 \text{ mW} \cdot \text{cm}^{-2}$  for systems with a PE sink and DPA annihilator,<sup>22</sup> and TTBP sink and A1 annihilator,<sup>24</sup> respectively.

For an ideal singlet sink, the  $I_{th}$  should be unaffected by the addition of a sink as FRET can only occur after the TTA event is complete. To understand the increase in  $I_{th}$ , the energy level of the first triplet excited state ( $T_1$ ) of PTEA was elucidated. Phosphorescence from PAHs is typically spin-forbidden, therefore the triplet energy level PTEA is difficult to probe using traditional fluorimetry techniques.<sup>44</sup> To ensure sufficient sensitization of the PTEA triplet level, higher concentrations of the dyes (sink and sensitizer) were necessary as compared to the concentrations used in previous UC films. PMMA films containing 10 wt% PTEA and 0.2 wt% PtOEP were melt-processed, after which the total photoluminescence emission of the films was measured at a temperature of 15 K (Figure S21a). Low-temperature spectroscopy revealed that  $T_1$  of PTEA is 1.57 eV. To compare, this is lower than the  $T_1$  values of PtOEP (1.92 eV) and DPA (1.72 eV), which is unexpected for such an efficient singlet sink.<sup>22</sup> It was previously theorized that a singlet-trapping sink could not be used if its  $T_1$  was lower than that of the annihilator, as this would promote premature depopulation of triplets before annihilation could occur.<sup>22,24</sup>

To address this question, we first examined the impact of low-triplet-energy sink on TTET efficiency from PtOEP to DPA with increasing PTEA concentration. By measuring PtOEP phosphorescence transients and evaluating TTET efficiencies, no change in  $\Phi_{TTET}$  ( $=87\%$ ) was observed with increasing sink concentration (Figure 9). This

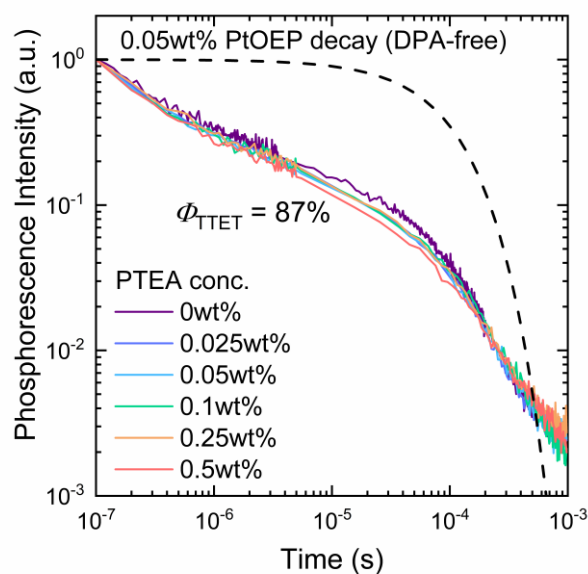


**Figure 9.** PtOEP phosphorescence transients measured at 645 nm upon excitation at 532 nm of melt-pressed PMMA films with 0.05 wt% PtOEP, 40 wt% DPA, and increasing concentration of PTEA.

indicates that the sink does not depopulate PtOEP triplets, which can be attributed to the relatively low concentrations of sink and sensitizer used in our UC films – thus limited number of PtOEP/PTEA active spheres.

As for the ability of PTEA to depopulate triplets from the annihilator after TTET, a potential signature for this phenomenon could be a reduction in annihilator triplet lifetime ( $\tau_T$ ), as suggested by the increase in  $I_{th}$  with rising sink concentration.  $\tau_T$  was assessed by measuring UC transients within the quadratic regime (Figure 10). Indeed, there was a noticeable trend toward a reduction in an overall UC lifetimes, coupled with an increase in  $I_{th}$ , which aligns well with Equation 2:

$$I_{th} = \frac{2(k_T)^2}{\gamma_{TTA} \alpha(E) \Phi_{TTET} \Phi_{ISC}} \quad (2)$$

where  $k_T$  is the triplet exciton decay rate ( $k_T = 1/\tau_T$ ),  $\gamma_{TTA}$  is the second-order TTA rate constant,  $\alpha(E)$  is the absorption coefficient of the sensitizer, and  $\Phi_{ISC}$  is assumed to be equal to 1. Sink-free upconverting films demonstrate an UC lifetime ( $\tau_{UC}$ ) of 1.32 ms, allowing for the derivation of  $\tau_T = 2 \times \tau_{UC} = 2.64$  ms (Figure S21b).<sup>45</sup> Increasing PTEA concentration accelerates UC decay, and at the highest PTEA load of 0.5 wt%, the  $\tau_{UC}$  is shortened to 0.83 ms. This decrease in  $\tau_{UC}$  significantly contributes to the observed increase in  $I_{th}$  at 0.5 wt% PTEA, given that  $I_{th} \approx (1/\tau_T)^2$ .<sup>22,41,42</sup> Thus, in this singlet-sink-type TTA-UC, the quadratic regime accounts for the spontaneous nonradiative decay of triplets on the annihilator, a process accelerated by the presence of the singlet sink. However, while triplet depopulation governs UC dynamics at excitation levels below  $I_{th}$ , above this threshold, the phenomenon of premature depopulation becomes unfavorable and does not contribute to the  $\Phi_{TTA}$  term, thus not affecting  $\Phi_{UC}$  (Equation 1).

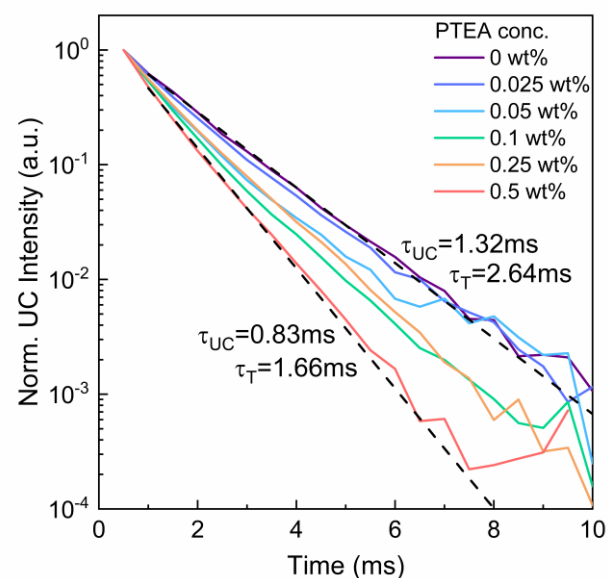


**Figure 10.** UC transients (in semi-log scale) of upconverting PMMA films with increasing PTEA concentration measured at peak emission wavelength. Excitation wavelength, 532 nm. Excitation density, below  $I_{th}$ . Dashed lines: exponential fits.

## Conclusion

While  $\Phi_{UC}$  has traditionally been deemed the paramount factor in designing high performing photon upconverting systems, the desire to expand TTA-UC to more robust applications necessitates improving solid-state UC emission intensity as well. In this work, we designed a novel blue-emitting singlet trapping sink, 9-phenyl-10-(*p*-tolylethynyl)-anthracene (PTEA), utilizing a relatively straightforward synthetic pathway and exhibiting  $\Phi_{FL}$  of 96% in dilute solution. By introducing PTEA to the benchmark upconverting PtOEP/DPA pair, we successfully limited parasitic back-FRET to the sensitizer at elevated concentrations, yielding  $\Phi_{UC}$  of 5% in bulk PMMA films containing PtOEP (0.05 wt%), DPA (40 wt%), and PTEA (0.25 wt%). Consequently, by augmenting the sensitizer load to 5 times higher than in previously studied analogous systems, we enhanced the intensity of both absorbed and emitted light within these rigid UC films.<sup>22,26,40</sup> Despite the lower  $T_1$  of the singlet sink compared to that of the annihilator, the utilization of low sink concentrations, facilitated by efficient forward-FRET{DPA→PTEA}, ensures the achievement of high  $\Phi_{UC}$ , albeit with a somewhat elevated UC threshold ( $I_{th} = 8$  mW/cm<sup>2</sup>). These results not only expand the scope of conceivable singlet sinks partnered with other sensitizer/annihilator pairs, but also further emphasize the contribution of singlet-sink-type TTA-UC to this evolving field.

## Author Contributions

Conceptualization: Y. C. S.

Data curation: S. T. S., S. R.

Formal analysis: S. T. S., S. R.

Funding acquisition: S. R., Y. C. S.

Investigation: S. T. S., S. R.

Methodology: S. T. S., S. R., K. K., Y. C. S.

Project administration: K. K., Y. C. S.

Supervision: Y. C. S.

Writing – original draft: S. T. S., S. R.

Writing – review & editing: K. K., Y. C. S.

## Conflicts of interest

There are no conflicts to declare.

## Acknowledgements

S. T. S. acknowledges support from the National Science Foundation Research Trainee (NSF NRT) Program Award #1449999. S. R. acknowledges funding by the European Social Fund (Project No. 09.3.3-LMT-K-712-23-0053) under a grant agreement with the Research Council of Lithuania (LMTLT). K. K. acknowledges the „Universities` Excellence Initiative”

programme by the Ministry of Education, Science and Sports of the Republic of Lithuania under the agreement with the Research Council of Lithuania (project No. S-A-UEI-23-6). Y. C. S. acknowledges support by the National Science Foundation under Grant No. 1757220

## References

- 1 C. A. Parker and C. G. Hatchard, *Proceedings of the Chemical Society*, 1962, **269**, 574.
- 2 C. A. Parker and C. G. Hatchard, *Transactions of the Faraday Society*, 1963, **59**, 284.
- 3 P. E. Keivanidis, S. Balushev, T. Miteva, G. Nelles, U. Scherf, A. Yasuda and G. Wegner, *Adv. Mater.*, 2003, **15**, 2095.
- 4 S. Balushev, F. Yu, T. Miteva, S. Ahl, A. Yasuda, G. Nelles, W. Knoll and G. Wegner, *Nano. Lett.*, 2005, **5**, 2482.
- 5 Y. C. Simon and C. Weder, *J. Mater. Chem.*, 2012, **22**, 20817.
- 6 Y. Zhou, F. N. Castellano, T. W. Schmidt and K. Hanson, *ACS Energy Lett.*, 2020, **5**, 2322.
- 7 S. Liu, H. Liu, Y. Hu, C. Zhao, H. Huang, G. Yu, Z. Li, Z. Liu, Y. Chen and X. Li, *Chem. Eng. Journal*, 2023, DOI:10.1011/866/j.cej.2022.139203.
- 8 S. Y. Hwang, D. Song, E. J. Seo, F. Hollmann, Y. You and J. B. Park, *Sci. Rep.*, 2022, DOI:10.1038/s41598-022-13406-8.
- 9 Y. Y. Cheng, B. Fückel, T. Schulze, R. W. MacQueen, M. J. Y. Tayebjee, A. Danos, T. Khoury, R. G. C. R. Clady, N. J. Ekins-Daukes, M. J. Crossley, B. Stannowski, K. Lips and T. W. Schmidt, *Organic Photovoltaics XIII*, 2012, **5**, 6953.
- 10 Y. Shang, S. Hao, C. Yang and G. Chen, *Nanomaterials*, 2015, **5**, 1782.
- 11 T. F. Schulze and T. W. Schmidt, *Energy Environ. Sci.*, 2015, **8**, 103.
- 12 F. Meinardi, M. Ballabio, N. Yanai, N. Kimizuka, A. Bianchi, M. Mauri, R. Simonutti, A. Ronchi, M. Campione and A. Monguzzi, *Nano. Lett.*, 2019, **19**, 2169.
- 13 A. Monguzzi, M. Mauri, A. Bianchi, M. K. Dibbanti, R. Simonutti and F. Meinardi, *J. Phys. Chem. C*, 2016, **120**, 2609.
- 14 X. Wang, R. Tom, X. Liu, D. N. Congreve and N. Marom, *J. Mater. Chem. C*, 2020, **8**, 10816.
- 15 T. N. Singh-Rachford and F. N. Castellano, *Coord. Chem. Rev.*, 2010, **254**, 2560.
- 16 T. Matsushita, T. Asada and S. Koseki, *J. Phys. Chem. A*, 2006, **110**, 13295.
- 17 J. Saltiel, G. R. March, W. K. Smothers, S. A. Stout and J. L. Charlton, *J. Am. Chem. Soc.*, 1981, **103**, 7159.
- 18 A. Monguzzi, R. Tubino, S. Hoseinkhani, M. Campione and F. Meinardi, *Phys. Chem. Chem. Phys.*, 2012, **14**, 4322.
- 19 S. Kobayashi, K. Kikuchi and H. Kokubun, *Chem. Phys. Lett.*, 1976, **42**, 494.
- 20 P. E. Keivanidis, S. Balushev, G. Lieser and G. Wegner, *Chem. Phys. Chem.*, 2009, DOI:10.1002/cphc.200900290.
- 21 V. Gray, K. Moth-Poulsen, B. Albinsson and M. Abrahamsson, *Coord. Chem. Rev.*, 2018, **362**, 54.
- 22 S. Raišys, S. Juršėnas, Y. C. Simon, C. Weder and K. Kazlauskas, *Chem. Sci.*, 2018, **9**, 6796.
- 23 N. Yanai and N. Kimizuka, *Chem. Comm.*, 2016, **52**, 5354.
- 24 T. Ogawa, M. Hosoyamada, B. Yurash, T. Q. Nguyen, N. Yanai and N. Kimizuka, *J. Am. Chem. Soc.*, 2018, **140**, 8788.
- 25 S. Raišys, O. Adomėnienė, P. Adomėnas, S. Juršėnas and K. Kazlauskas, *Dyes Pigm.*, 2021, DOI:10.1016/j.dyepig.2021.109565.
- 26 S. Raišys, S. Juršėnas and K. Kazlauskas, *Solar RRL*, 2022, DOI:10.1002/solr.202100873.
- 27 R. Vadrucchi, C. Weder and Y. C. Simon, *J. Mater. Chem. C*, 2014, **2**, 2837.
- 28 J. C. de Mello, H. F. Wittmann and R. H. Friend, *Adv. Mater.*, 1997, DOI:10.1002/adma.19970090308.
- 29 R. Martin and S. L. Buchwald, *Acc. Chem. Res.*, 2008, **41**, 1461.
- 30 T. Chidanguro, D. R. Blank, A. Garrett, C. M. Reese, J. M. Schekman, X. Yu, D. L. Patton, N. Ayres and Y. C. Simon, *Dalton Trans.*, 2018, **47**, 8663.
- 31 V. Gray, A. Dreos, P. Erhart, B. Albinsson, K. Moth-Poulsen and M. Abrahamsson, *Phys. Chem. Chem. Phys.*, 2017, **19**, 10931.
- 32 Q. Li and Z. Li, *Adv. Sci.*, 2017, **4**, DOI:10.1002/adv.2016004.
- 33 W. Jiang, Y. Shen, Y. Ge, C. Zhou, Y. Wen, H. Liu, H. Liu, S. Zhang, P. Lu and B. Yang, *J. Mater. Chem. C*, 2020, **8**, 3367.
- 34 T. Schillmöller, R. Herbst-Irmer and D. Stalke, *Adv. Opt. Mater.*, 2021, DOI:10.1002/adom.202001814.
- 35 S. Raisys, O. Adomėnienė, P. Adomėnas, A. Rudnick, A. Kohler and K. Kazlauskas, *J. Phys. Chem. C*, 2021, **125**, 3764.
- 36 R. Karpicz, S. Puzinas, V. Gulbinas, A. Vakhnin, A. Kadashchuk and B. P. Rand, *Chem. Phys.*, 2014, **429**, 57.
- 37 S. H. Lee, D. C. Thévenaz, C. Weder and Y. C. Simon, *J. Polym. Sci., Part A: Polym. Chem.*, 2015, **53**, 1629.
- 38 S. H. Lee, J. R. Lott, Y. C. Simon and C. Weder, *J. Mater. Chem. C*, 2013, **1**, 5142.
- 39 S. H. Lee, M. A. Ayer, R. Vadrucchi, C. Weder and Y. C. Simon, *Polym. Chem.*, 2014, **5**, 6898.
- 40 S. Raišys, K. Kazlauskas, S. Juršėnas and Y. C. Simon, *ACS Appl. Mater. Interfaces*, 2016, **8**, 15732.
- 41 A. Haeefele, J. Blumhoff, R. S. Khnayzer and F. N. Castellano, *J. Phys. Chem. Lett.*, 2012, **3**, 299.
- 42 A. Monguzzi, J. Mézyk, F. Scotognella, R. Tubino and F. Meinardi, *Phys. Rev. B.*, 2008, **78**, 195112.
- 43 F. Edhborg, A. Olesund and B. Albinsson, *Photochem. Photobiol. Sci.*, 2022, **21**, 1143.
- 44 J. V. Goodpaster, J. F. Harrison and V. L. McGuffin, *J. Phys. Chem. A*, 2002, **106**, 10645.
- 45 A. Köhler and H. Bässler, *Mater. Sci. Eng., R*, 2009, **66**, 71.
- 46 Y. Gao, J. Zhang, J. Liang, D. Yuan and W. Zhao, *Eur. Polym. J.*, 2022, **175**, 111379.